Astron. Astrophys. 320, 811–822 (1997)

ASTRONOMY
AND
ASTROPHYSICS

A further look into the pulsating PG1159 stars

Alfred Gautschy

Astronomisches Institut der Universität Basel, Venusstr. 7, CH-4102 Binningen, Switzerland

Received 18 June 1996 / Accepted 2 October 1996

Abstract. To improve our understanding of the pulsational instabilities found in some of the PG1159-type pre-white dwarfs we performed detailed nonradial stability analyses on helium-star evolutionary models. Adopting canonical chemical compositions as derived from spectroscopic observations, we found pulsational instabilities for all stellar masses considered (0.57, 0.63, 0.7 $M_\odot$). The blue boundary of the instability domain agrees satisfactorily with observations. The red edge, on the other hand, is found to extend to lower temperatures than presently admitted by observations. The dependence of the pulsational instabilities on helium or even hydrogen abundance in the stellar envelopes is found to be less stringent than emphasized hitherto. In particular, we obtained pulsationally unstable g modes for model stellar envelopes which are representative for HS2324+3944 – a newly discovered PG1159-star with a hydrogen abundance X = 0.2 and which is claimed to be pulsating.

Key words: stars: oscillations – stars: white dwarfs – stars: interiors

1. Introduction

The hottest stars we know are those passing through the post-asymptotic giant-branch (post-AGB) evolutionary phase; they are shortly before settling onto the cooling sequence as white dwarfs. The corresponding stellar evolutionary tracks are characterized by a pronounced 'knee' joining the evolution at almost constant luminosity with one at roughly constant radius (cf. Fig. 1). Spectroscopic observations show that some of these stars are essentially devoid of hydrogen but with strong helium, carbon, and oxygen features (see e.g. Dreizler et al. 1995). This class of stars is named after PG1159-035. About 50 % of the 32 known PG1159 stars are surrounded by planetary nebulae and can be considered as direct descendants of recent leavers of the AGB. The PG1159 objects lacking evidence of an associated nebulosity cannot be attributed unambiguously an evolutionary state.

Some PG1159 stars are photometrically variable with periods ranging from 10 to about 30 minutes. They are termed GW Vir or DOV variable stars – we will use the first name in the following. Nine such variables are presently known. The high-luminosity members of the class have about four times longer periods than those being close to the white dwarfs' cooling tracks. The longer-period PG1159 stars are usually variable central stars of planetary nebulae and are referred to as PNNVs or variable CSPNe in the literature. Since there are also cooler variable central stars it is necessary to emphasize that we consider here the *hot* PNNVs with $T_{\rm eff}$ around 10^5 K. The purpose of this paper is to look into the pulsation-mode physics acting in PG1159 stars. We will not distinguish between the high- and the low-luminosity branch during the stellar evolution since the excitation/damping physics of the oscillation modes should remain unaltered. Hence, in the following discussions it is not important whether a GW Vir variable is surrounded by a planetary nebula or not. For aspects of evolution and/or population statistics in the instability region, however, the very presence of a planetary nebula might very well help to discern between different scenarios.

The GW Vir variability is attributed to the overstability of low-degree, high-order gravity (g) modes. The observed frequency spectra are quite rich – i.e. many modes are excited simultaneously – and they are used with considerable success for seismological analyses (e.g. Kawaler & Bradley 1994). As an example, based on the data of one of the 'Whole Earth Telescope' observing campaigns, the power spectrum of the variability of PG1159-035 itself allowed the resolution of 125 individual frequencies (Winget et al. 1991). For seismological studies *per se*, the excitation physics of the pulsation modes is irrelevant. The results from adiabatic oscillation computations – neutrally stable oscillations modes – suffice to identify and interpret the observed peaks in the power spectra. Irregularities in the distribution of the oscillation frequencies serve as a tool to probe aspects of the internal structure of the oscillating stars. The main objective of seismological studies is to constrain the stratification of the stellar envelopes and to accurately measure global stellar parameters which are not directly accessible otherwise.

The physical origin of the pulsational instability of GW Vir-type was addressed in the middle of the 1980s by Starrfield et al. (1984, 1985). They identified the partial K-shell ionization of carbon and/or oxygen as the destabilizing agent. Due to the rather weak opacity bump produced by this ionization stage, even minor contamination of the stellar matter by ele-

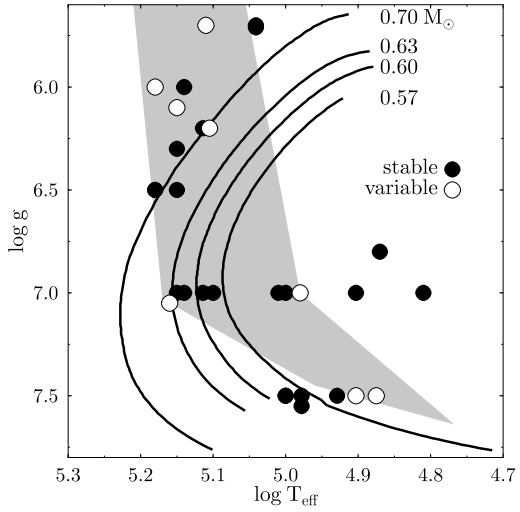

Fig. 1. The observed distribution of some of the PG1159-035 stars on the $T_{\rm eff}$ – $\log g$ plane. Solid dots show the spectroscopic calibration of photometrically stable stars. The white circles indicate the GW Vir variables and the hot, variable central stars of planetary nebulae (hot CSPNe). The solid lines derive from our stellar evolution calculations of helium stars which were performed for this study. The grey area covers the observationally defined instability domain of PG1159 stars.

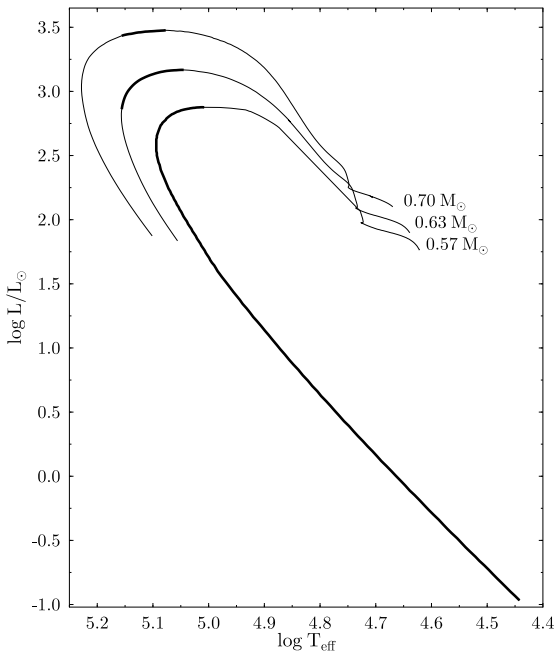

Fig. 2. Loci of the initially chemically homogeneous helium stars with 0.57, 0.63, and $0.70 M_\odot$ on the HR diagram. Stability analyses were performed on models that had passed the maximum luminosity. The structure of the envelopes of such models resembles that of models coming directly from the AGB and having lost their H-rich envelope by some mechanism. The overlaid heavy lines indicate regimes where pulsationally overstable ℓ = 1 modes were found.

ments other than C and O were found to effectively destroy the pulsational instabilities. In particular, H and He had to be banished from the excitation region which had to be assumed to be made up of mixtures of C and O only in the studies of Starrfield et al. (1984, 1985). A marginal instability region on the high-, constant-luminosity side of the evolutionary knee – appropriate for variable hot CSPNe – was obtained with a helium mass fraction of 0.1 in Stanghellini et al. (1991). Higher helium abundances led to a shrinking of the instability domain, covering only the white-dwarf cooling tracks, so that they could be ruled out to explain *any* hot pulsators of GW Vir type, i.e. variables with $T_{\rm eff} \gtrsim 10^5$ K.

Since the GW Vir variables are few a reliable observational determination of the borders of the instability region is difficult and probably still rather unreliable. An attempt was presented recently by Werner et al. (1995) and it was used to delineate the instability region in Fig. 1. Notice that the border suggested by Werner et al. continues to lower $\log g$ values than shown in Fig. 1; this region is not of interest here since the most massive star we consider has $0.7 M_\odot$.

Recently, Saio (1996) reviewed the pulsation properties of hydrogen-deficient stars. Among others, he also dealt with GW Vir variables and hot, variable CSPNe. Using the new generation opacity data (the OPAL brand in his case) he encountered pulsational instabilities for chemical compositions for which only stable modes were identified when the old opacity tables were adopted. Saio's computations suggest that the previously stringent chemical composition constraints for pulsational instabilities need to be relaxed. He presented also a period – $T_{\rm eff}$ diagram which overlaps satisfactorily with observational data.

Another theoretical study addressing the GW Vir variability was published very recently by Bradley & Dziembowski (1996). From their nonadiabatic computations they concluded that these pulsators must have oxygen-rich driving regions, with a corresponding relative mass abundance that must exceed 50 %. Otherwise, the periods of the maximum unstable modes were too short compared with observations. As a further way out, Bradley & Dziembowski suggested a significant, non-standard increase of the stellar radii compared with stellar evolution results.

A major unresolved problem is posed by the observation that even if a PG1159 star lies in the instability region, lets say on the $\log T_{\rm eff}$ – $\log g$ plane, this does not compulsively imply its variability. Only about half of the population of the known PG1159 stars inside the instability domain pulsates. The dilemma intensifies when we realize that spectroscopic twins are observed of which one is variable and the other is stable (Werner et al. 1991).

This paper presents a nonradial, nonadiabatic survey of low-degree g modes in GW Vir-like stars using OPAL opacity data for the radiative opacities. The modeling methods are described in Sects. 2 and 3. In Sects. 4 and 6, we emphasize aspects of stellar and mode physics and to some degree the influence of chemical composition; this is done mainly on a qualitative level rather than attempting to fit particular observations. One exception is the star HS2324+3944 which is a recently discovered

PG1159 star with measurable amounts hydrogen in its spectrum *and* which additionally is claimed to be pulsating (Silvotti 1996). Sect. 5 deals with our modeling of this object.

2. Construction of the PG1159 models

The stellar models on which we performed the stability analyses were obtained from stellar evolution computations. Hence, we could analyze the nonradial oscillations on complete stellar models. The applied finite-difference scheme solves the structure/evolution equations of a star from the center to the photosphere. The physical processes accounted for in the code are those described in the paper of Gautschy et al. (1996). In particular, we point out that He, C, *and* O ionization are accounted for in the equation of state (EoS). All regions of the stellar interior are treated with the identical formulation of the EoS to avoid discontinuities in thermodynamical quantities at switching points of the formulations. Convection was dealt with in the standard MLT approach with a mixing length of 1.5 pressure scale heights. For the very hot stars in which we are interested here the particular formulation of convective energy transport should not be very crucial. Opacity data were taken from the freely accessible C and O enhanced OPAL repository (in its 1992 version) at Livermore (called $\kappa_{\rm table}$). At very high temperatures, above 10^8 K, the tables were frequently not broad enough in the R variable to accommodate the stellar interiors. In this high-temperature domain we extended the tables with approximations from analytical formulae (called $\kappa_{\rm analyt.}$) that were described in Gautschy et al. (1996). To avoid jumps in the Rosseland mean we defined an ad-hoc overlap region in temperature over which we switch linearly, according to $\theta \times \kappa_{\rm table} + (1-\theta) \times \kappa_{\rm analyt.}$, between the two approaches. The transition width spanned usually 10^6 K. To make best use of the OPAL data we also implemented their interpolation code (`cotrin`) to interpolate within a single opacity table as well as between different chemical compositions for a fixed amount of hydrogen. Concerning nuclear combustion, we treated burning of He to C, O, and Ne. Energy losses by neutrinos were included using the fits of Munakata et al. (1985). Elemental diffusion in the strong gravitational field that builds up after passing the evolutionary knee was not included in the calculations.

Our model series started as homogeneous helium main-sequence stars with a composition compatible with observed surface abundances in PG1159 stars. Except if noted otherwise, we used X = 0, Y = 0.38, C = 0.4, O = 0.2. Fig. 2 shows the evolutionary tracks of the three stellar masses ($0.57, 0.63$ and $0.7 M_\odot$) which were evolved for the purposes of this study. The chemically homogeneous helium zero-age main-sequence models were followed as far as possible through the core and shell helium burning. During the He shell-burning episode the He-star models close in to post-AGB tracks of originally H-rich 'canonical' stellar models. By the time the effective temperature has risen to about 10^5 K the position of the He stars on the Hertzsprung-Russell (HR) diagram and their envelope structure (such as temperature and density gradients) are comparable with results from canonical stellar evolution.

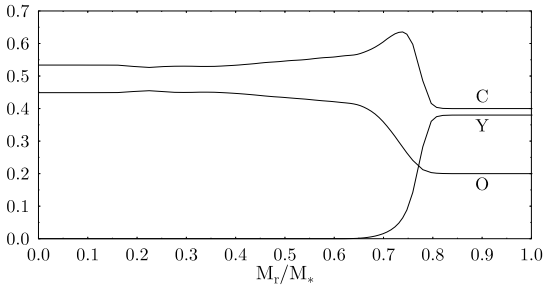

Fig. 3. Example of the chemical stratification of a $0.7 M_\odot$ model at the luminosity maximum of its evolutionary track which is depicted in Fig. 1.

Fig. 1 shows that the He-star evolutionary tracks (at least for phases after the luminosity maximum) match reasonably well with standard evolutionary tracks on the $\log T_{\rm eff} - \log g$ plane by the time they cross the GW Vir instability domain. The comparison was made with the collection from the literature of standard, originally hydrogen-rich stellar evolution tracks shown in Dreizler et al. (1995). Fig. 2 shows the corresponding evolutionary tracks on the HR diagram. The locus of our $0.6 M_\odot$ star on the $\log g - T_{\rm eff}$ plane in Fig. 1 is the result of early test computations and was not used for nonradial oscillation analyses.

The two most massive evolutionary sequences run out of the opacity tables at the rather low temperatures of a few times 10^7 K shortly after they passed the evolutionary knee. Due to the lack of a suitable extension of opacity data at such low temperatures we stopped the computations there. Only the $0.57 M_\odot$ could be followed quite far down the cooling track. We terminated the computation of its evolution after the effective temperature fell below 50 000 K at a luminosity of $1.7 L_\odot$.

A representative spatial run of the chemical stratification of a He star model is displayed in Fig. 3. It belongs to the $0.7 M_\odot$ model at the luminosity maximum in the HR diagram. The burning shell starts at about $0.8 M_*$. Within about a tenth of the stellar mass all the helium is burned away. When the evolution proceeds the shell burns further into the stellar envelope. Except for a translation, the functional form of the abundance profile does not change significantly. The same applies when considering different stellar masses. In the particular case of the $0.57 M_*$ model which we were able to follow to low luminosities the size of the nuclearly unprocessed envelope shrinks to about $4.6 \times 10^{-2} M_*$ at $20 L_\odot$.

The evolutionary history behind *our* GW Vir models is very different from that emerging from canonical – originally hydrogen-rich – stellar models. Their evolution through the AGB, in particular, opens a huge, ill-constrained parameter space to force the star to lose its hydrogen-rich envelope until it arrives at the domain of the GW Vir variables. In contrast to earlier believes (e.g. Paczyński 1970), Blöcker (1993) showed that the structure even of the degenerate cores of AGB leavers depend on the computational assumptions put to work during the preceding evolutionary phases. Since we are still lacking self-consistent descriptions for mass-loss and the AGB-

termination process in particular a fully trustworthy approach which should be applied to deal with this evolutionary stage has not yet emerged.

From what we said in the last paragraph it follows that also the time-scale of the post-AGB evolution depends on the computational particularities that entered the earlier evolution of a stellar model. However, stellar models regain thermal equilibrium to a good degree shortly after leaving the AGB (Schönberner 1983). Therefore, even if the evolutionary speed were wrong, the physical stratification of the envelopes which shape the characteristics of the g modes is not strongly influenced by the evolutionary history of the star. This aspect is also supported by the ability to compute g modes of GW Vir variables with static envelope models only (Bradley & Dziembowski 1996).

Compared with stellar models which suffered – essentially ad hoc specified – mass loss during and shortly after the AGB phase our models show He envelopes that are up to a factor of ten thicker. This difference is essential when discussing mode trapping (see Sect. 6 and 7). Mode stability, however, is not believed to be influenced significantly.

3. Nonradial nonadiabatic oscillation treatment

The nonradial, nonadiabatic stellar oscillation code use was described in the paper of Gautschy et al. (1996). Nuclear terms were included here for the sake of completeness. As only helium burning was considered, equilibrium treatment of the ϵ-mechanism was sufficient. The boundary conditions in the center are dictated by the regularity of the perturbations of the physical quantities. At the surface we assume that the Stefan-Boltzmann law for radiation obtains and full reflection of the waves as the mechanical boundary condition. Convection was always treated as being frozen-in, i.e. the perturbation of the convective flux was assumed to be negligible. In most of the hot models the particular treatment of convection might be irrelevant due to its marginal contribution to the energy transport. The eigenvalues $\sigma = (\sigma_{\rm R}, \sigma_{\rm I})$, where $\sigma_{\rm R}$ stands for the oscillation frequency and $\sigma_{\rm I}$ for the excitation/damping rate, are always expressed in units of $\sqrt{3GM_*/R_*^3}$.

4. Results from stability analyses

In this section we present the results of nonradial, nonadiabatic pulsation computations performed on $0.7, 0.63$, and $0.57 M_\odot$ evolutionary sequences. Each of the model series will be dealt with separately. We start by discussing the obtained *modal diagrams* (plot of period vs. some control parameter such as $\log g$) and consequences therefrom. Mostly, mode computations were restricted to $\ell = 1$ g modes.

First we turn to the most massive star sequence – the $0.7 M_\odot$ models. Fig. 4 shows the variation of the periods of some of the $\ell = 1$ g modes as evolution proceeds. The star's evolution is parameterized by its surface gravity which monotonically increases as evolution proceeds.

The upper panel of Fig. 4 shows the variation of the periods of some g modes as the star evolves around the knee. A

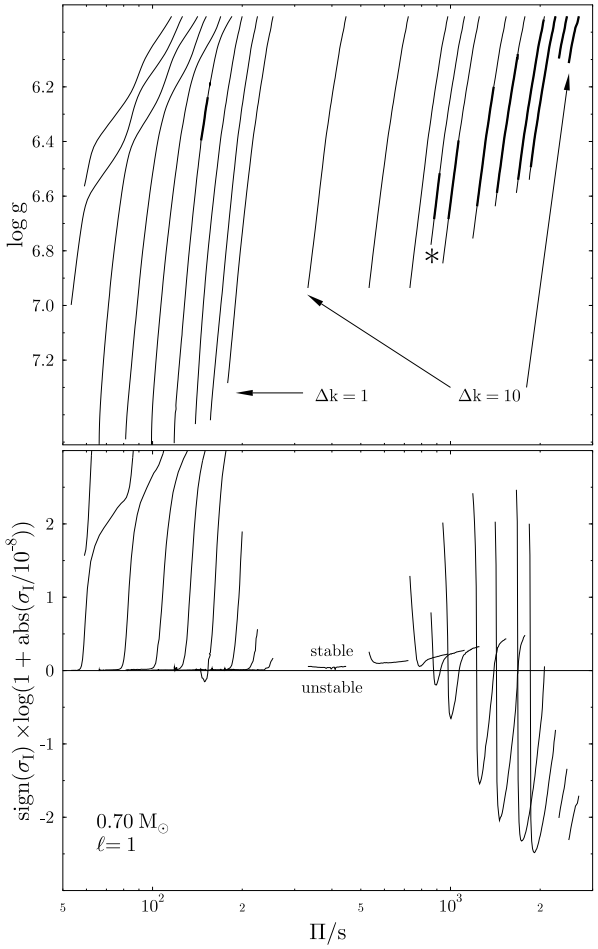

Fig. 4. Modal diagram of the lower-order, $\ell = 1$ g modes of the last part of the $0.7 M_\odot$ sequence. Top panel: Light lines trace the variation of the oscillation periods of particular overtones as the surface gravity changes during the evolution. Unstable regimes are marked by thick lines. The short-period modes are separated by $\Delta k = 1$ up to the mode pointed to with the appropriate arrow. The long-period modes are, as indicated with the other arrows, separated by $\Delta k = 10$. An exception is the mode with the asterisk. Its neighboring modes are separated by $\Delta k = 5$. Bottom panel: The variation of the imaginary parts of the modes. Due to the large range spanned by the imaginary parts the scaling is logarithmically for values much larger than 10^{-8}.

particular radial order (denoted by k) is traced by a thin line. Since we were dealing with high-order modes, only a small fraction of the radial orders within the period span relevant for GW Vir variables was followed. In this respect, the upper panel can be divided again. In the low-period domain – between about 50 and 200 s – we computed the eigenvalues of every radial order. Above about 300 s – in the long-period regime – only every 10th radial order (region between the arrows originating from $\Delta k = 10$ in Fig. 4) was followed. The only exception, with a period separation of $\Delta k = 5$ to both sides, is marked with an asterisk. For easier identification of the instability domains, the pulsationally unstable mode branches are traced with heavy lines. From the lower panel in Fig. 4 we see this to cor-

respond with negative $\sigma_{\rm I}$ values in our sign convention of the eigenvalues. For better graphical presentation we appropriately scaled the large numerical range of the imaginary parts. Moduli of $\sigma_{\rm I}$ exceeding 10^{-8} scale logarithmically in this choice of the ordinate. Smaller values behave essentially linear. The sign function allows to discern between damped and overstable oscillation modes.

The short-period domain in Fig. 4 shows sequences of avoided crossings occurring in low-order modes of the low surface-gravity models. The avoided crossings appear in period as well as in the imaginary parts of the eigenfrequencies. A local analysis of the first model of the series shows that eigenmodes with periods below about 220 s have dual character. Deep in the interior they propagate as *g* modes and as *p* modes in the envelope. The less steep portions of the eigenmode branches involved in the avoided crossings reflect the different reaction on the stellar evolution of the *p*-mode propagation speed in the envelopes. Away from avoided crossings, the less steep branches correspond to modes which are dominated by the *p*-mode cavity. In accordance with a strong coupling with the envelope of the short-period modes early in our evolutionary phases they have, compared with core-dominated *g* modes, high damping rates which are induced by considerable radiative damping in the envelopes. Fig. 4 shows imaginary parts as high as 10^{-5} only. The maximum $\sigma_{\rm I}$ values encountered rise to about 10^{-3}.

For a short phase of the evolution, one of the short-period modes turns weakly pulsationally unstable. The period ranges from 145 to 152 s. The excitation rate is very low as can be seen in the lower panel of Fig. 4. We ensured its reality by reiterating this mode several times with different accuracy bounds for the numerical scheme and with different start-guesses for the eigenvalue. Repeated convergence to this weak instability proved that we can confirm the pulsational instabilities at short periods which were also seen by Saio (1996, his Fig. 5). The instability is induced by the He-burning shell through the action of the ϵ-mechanism. Only a very narrow period range and a short evolutionary phase are prone to such instabilities. In the $0.7M_\odot$ star models this leads to one radial order only which can be weakly destabilized at $\ell = 1$. The radial displacement eigenfunction of the unstable mode has 5 nodes within the *g*-mode cavity and none in the acoustic propagation region. The maximum growth rate of the nuclearly destabilized *g* mode amounts to an e-folding time of 1.5×10^3 y. The star's evolution through this instability phase lasts about 10 times longer in our computational approach. This might be marginally sufficient for an ϵ-destabilized mode to build up. In comparison with the long-period *g*-mode instabilities, the instabilities effected by the ϵ-mechanism appear to be hardly of relevance.

In the long-period domain, where modes have always pure *g*-mode character, pulsational instabilities occur for periods longer than 880 s (cf. Fig. 4). The higher the radial order of the modes the lower the surface gravity at which instability shows up. The locus of the mode marked with '$*$' has $k = 45$. It was inserted in the usual $\Delta k = 10$ sequence to more accurately determine the low-period border of the instability region. Fig. 4 shows a small fraction only of all the modes that are be pulsationally unstable. To find the highest overstable overtone we restricted the computations to the first stellar model of the series. The longest-period unstable mode which was found in the $0.7M_\odot$ sequence lies at about 7447 s. This is a truly remarkable range of simultaneously unstable radial orders. Since the Riccati method does not in general involve the simultaneous computation of the eigenfunctions when relaxing eigenfrequencies we had to estimate the range of covered radial orders by applying the asymptotic *g*-mode period separation formula. For the model at $\log g = 5.94, \log T_{\rm eff} = 5.045$, and $\ell = 1$ we deduce about 200 modes to be simultaneously overstable. Over most of the unstable period range, the imaginary parts remain at $\sigma_{\rm I} = \mathscr{O}(10^{-6})$. The return to stability of the very-high overtones appears rather abruptly.

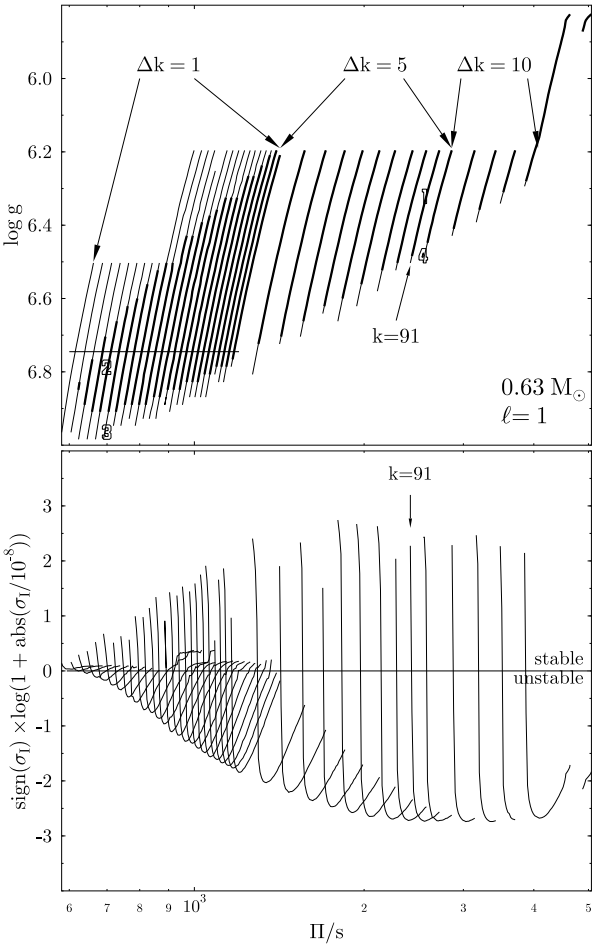

Fig. 5. Same as Fig. 4 but for the $0.63M_\odot$ series. The outlined numbers are locations where different spherical degrees were computed; they are discussed in Sect. 6. The horizontal line at $\log g = 6.745$ indicates the position at which period separations and the variation of the imaginary parts of eigensolutions of subsequent radial orders were computed (see Fig. 11).

The models of the $0.63M_\odot$ evolutionary track were processed similarly as those of the $0.7M_\odot$ sequence. The resulting $\ell = 1$ modal diagram is shown in Fig. 5. Only the modes rele-

vant for the eventually uncovered instability region are shown. The modal analysis of the $0.63M_\odot$ models is the most dense one – in terms of covered radial orders – of this project. The radial-order spacing between the displayed lines is labeled in the top panel of Fig. 5.

As in the $0.70M_\odot$ case, the instability region has an expressed finger-like shape pointing from low-log g and long periods to high-log g and short periods. The high-log g edge of the instability region lies at about log g = 6.85. The hottest point of the $0.63M_\odot$ evolutionary track is reached at log g = 7.0. Hence, the instability domain terminates before the $0.63M_\odot$ models start to dim and before they approach the white dwarf cooling sequence. As far as $0.7M_\odot$ computations could be continued (cf. Fig. 1) we found no return to pulsational instability.

Again, a large number of radial overtones remained overstable also in the earliest model of the sequence. Therefore, we stopped the tracking of particular radial orders around 5000 s. The very smooth and stretched ridge in $\sigma_{\rm I}$ is seen in Fig. 7's lower panel. The highest-order ℓ = 1 mode which was found overstable at log g = 5.83 (i.e. the first model) has a period of about 9500 s. In contrast to classical pulsators such as Cepheids or RR Lyrae stars, a large number of radial overtones appear to be simultaneously favored for excitation.

The locus of the k = 91 dipole mode is marked in Fig. 5. This mode serves to count the radial orders of the other plotted modes and it emphasizes the high order of the excited modes. The number of nodes was counted in the displacement eigenfunction. This particular mode was chosen because it belongs to the maximum excited ones in the $0.63M_\odot$ sequence. We return to in Sect. 6.

The lowest-mass evolutionary sequence considered here had $0.57M_\odot$. The results from the nonadiabatic eigenanalyses for ℓ = 1 are shown in Fig. 6. In contrast to the before-mentioned sequences, the instability domain extends beyond the knee into the white dwarf cooling stage. Therefore, we indicated the log g value at which the highest effective temperature was reached by a horizontal line in Fig. 6. For economic reasons we restricted ourselves to a rather coarse coverage of the period domain. The low-period range ($\Pi \lesssim 800$ s) was scanned with Δk = 5 until we reached that radial order which did not become overstable in the whole model series. At long periods, we stopped tracking the modes along the model series after the first model of the $0.57M_\odot$ sequence turned pulsationally unstable. For longer periods we stayed with the first model for which we searched for the longest overstable mode. It was found at about 5500 s.

The long-period 'instability finger' is also contained in Fig. 5. It merges, however, with a short-period instability domain which extends to low luminosities and hence late evolutionary stages. Periods as short as 300 s become overstable. The ℓ = 1 g modes of the last model of the $0.57M_\odot$ evolutionary sequence were all pulsationally stable again. Hence, the red edge on the low-luminosity branch lies at log $T_{\rm eff}$ = 4.45 and log $L/L_\odot = -0.1$. In our computations there is one radial order which becomes pulsationally overstable at high luminosities and again – after a phase of stability – at low luminosities.

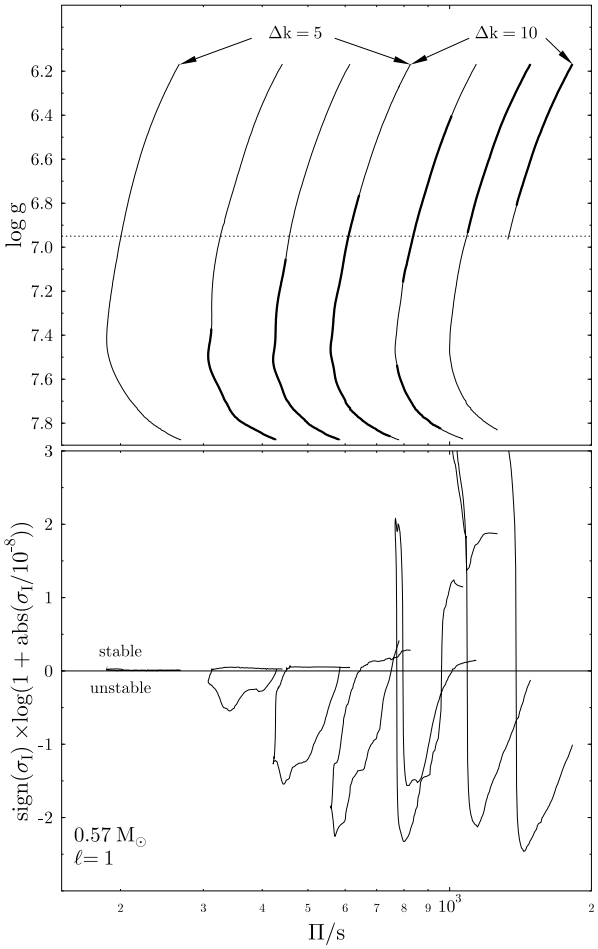

Fig. 6. Same as Fig. 4 but for the $0.57M_\odot$ series. The dashed horizontal line marks the hot-most point of the evolutionary knee. For higher surface gravities the star approaches the white dwarf cooling tracks.

The lower panel of Fig. 6 shows the variation of the imaginary parts of the eigenfrequencies. The high-luminosity part is smooth and looks very similar to the results of the more massive star sequences. The low-luminosity imaginary parts are, despite their comparable magnitude, less smooth. This is not numerically caused. At low luminosities the transition from the He-rich envelope to the pure CO core is rather steep and as close to the surface as it can ever come. Therefore, the g modes are partially reflected at the composition transition such that trapping of modes is expected. Such mode trapping shows also up in the imaginary parts of the eigenfrequencies (cf. Gautschy et al. 1996) leading to the 'bumpy' appearance.

We notice finally that the extension of the instability with respect to radial orders is much narrower at low luminosities than on the high-luminosity branch. The envelope covering the short-period $\sigma_{\rm I}$ peaks in the lower panel of Fig. 6 crosses zero at a very steep angle at about 1000 s. This is much different from the behavior of the envelope over the $\sigma_{\rm I}$ curves in larger-mass sequences for which the long periods are unstable only on the high-luminosity branch of the evolutionary track.

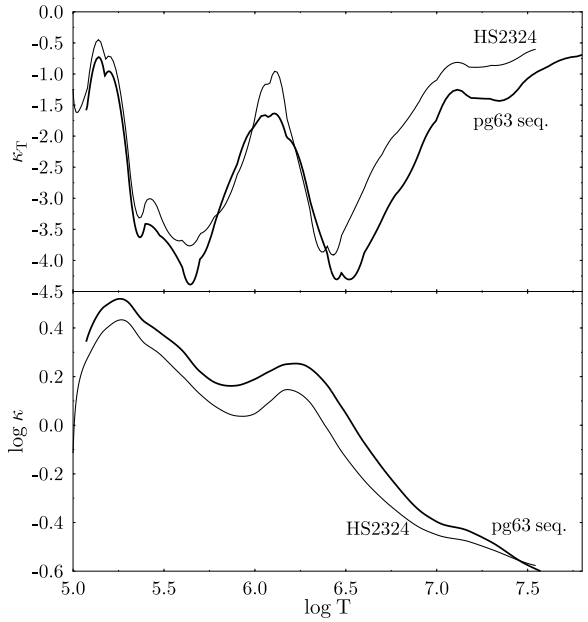

Fig. 7. Comparison of pulsationally interesting physical quantities between $0.63 M_\odot$ He star models (pg63 seq.) and envelope models for HS2324. The HS2324 models differ in their chemical composition, in particular the under-abundance in O compared with the evolutionary sequences. Top panel: logarithmic opacity derivative with respect to temperature at constant density. Bottom panel: spatial run of the logarithm of the opacity. The depth in the stellar envelopes is parameterized by the temperature.

5. The peculiar case of HS2324+3944

Dreizler et al. (1996) reported the discovery and spectroscopic analysis of the peculiar PG1159 star HS2324+3944. In contrast to the other members of this class it shows an atmospheric ratio (by number) of He to H of 0.5. Furthermore, HS2324 shows an unusual low oxygen abundance. In mass fractions, we adopt X=0.2, Y=0.41, C=0.37, O=0.01 (Werner, private communication). Recently, Silvotti (1996) provided first observational results indicating that HS2324 is a GW Vir-type variable with a dominant period of about 2140 s. According to previous nonradial stability analyses (e.g. Starrfield et al. 1984) any trace of hydrogen was considered to poison pulsational instabilities.

The spectroscopic calibration places HS2324 at about $\log g = 6.2$ and $\log T_{\rm eff} = 5.11$ (Dreizler et al. 1996). Based on the loci of our helium-star models in the $\log g$ – $\log T_{\rm eff}$ plane, we assumed a stellar mass of $0.63 M_\odot$, this is slightly larger than what Dreizler et al. proposed. We constructed stellar envelope models with homogeneous chemical composition adopting abundances as mentioned in the last paragraph. The integration starting at the stellar surface extended to the onset of significant hydrogen burning at about 3×10^7 K.

The bottom panel of Fig. 7 shows clearly the decrease of the opacity in the envelope models with HS2324 composition when compared with the evolutionary helium-star models. At the same time, the opacity bump around $\log T = 6.25$ appears to become narrower. Hence, pulsational driving is not expected to be significantly weakened by neither the existence of hydrogen nor the suppressed oxygen abundance. The $\kappa_{\rm T}$ slope in both stellar models (HS2324 envelope and evolutionary He-star) are comparable (cf. top panel of Fig. 7). Actually, the slope in the HS2324 model appears to be marginally steeper than in the full He-star model.

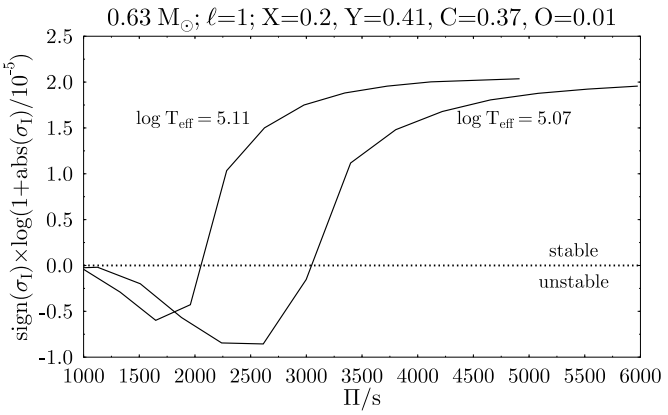

Fig. 8. Appropriately scaled imaginary parts of eigenfrequencies as a function of period of $\ell = 1$ g modes. The two curves show the results of two different choices of the stellar models' $T_{\rm eff}$ both at $\log L/L_\odot = 3.16$.

5.1. The pulsation properties of HS2324

As for the full helium-star models, we performed eigenanalyses on the envelope models for HS2324. The inner boundary of the envelope was treated as a reflective wall. This influences the period spacing between adjacent orders of the computed g modes only. In the cases considered the spacing was about five times larger than for full $0.63 M_\odot$ models with comparable effective temperature. The magnitude of the work integrals are not expected to be much different. Most of driving and damping occurs at temperatures below $\log T = 6.5$. In our modeling of HS2324 we miss some dissipation from the deep interior. The Brunt-Väisälä frequency achieves its maximum close to the center so that the eigenfunctions have there their most rapid spatial oscillations. From the full models we derive that only a few percent of the total work is done in the deep interior. Our imaginary parts are hence expected to be marginally too large. The qualitative behavior is, however, believed to be correct.

Fig. 8 displays the imaginary parts of low-order $\ell = 1$ g modes for two different envelope models. Obviously it is possible – also with a considerable hydrogen admixture of 20 % in mass – to obtain pulsational instabilities for HS2324-like stellar envelopes. Fig. 8 shows that the destabilized period range depends markedly on the choice of effective temperature. Based on the results for $\ell = 1$ and the observed period of the variability we tend to favor a temperature closer to $\log T_{\rm eff} = 5.07$ which is lower – but still within the limits of uncertainty – than suggested by Dreizler et al. (1996).

As Fig. 8 clearly shows, the period domain over which dipole modes become pulsationally unstable is much narrower

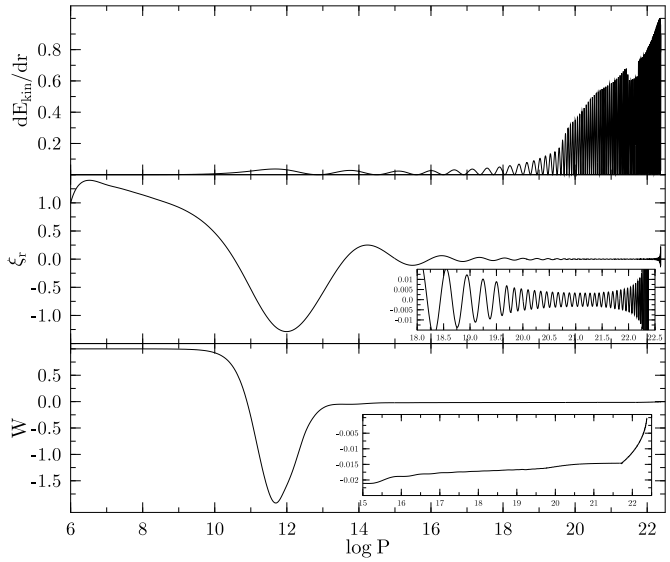

Fig. 9. Work integral and normalized radial displacement of the nonadiabatic eigensolution for $k = 91, \ell = 1$ of the $0.63 M_\odot$ model at $\log g = 6.43$. This mode belongs to the most unstable ones encountered. Blow-ups of the central behaviors in displacement and contributions to the work integral are shown as small inlets.

in the HS2324 models than in the hydrogen-free and oxygen-rich helium-star models. The excitation rates are comparable in both cases. Hence, it is not at all surprising if pulsations develop – as they do in 'classical' GW Vir variables – in HS2324-like objects. The frequency spectrum must be expected to be poorer, however.

6. Discussion

In the following we take a closer look at the properties of the computed eigensolutions and the physical properties of the driving behind GW Vir-type instability.

The high quality of the nonadiabatic eigensolutions which was achieved in this study can be seen in Fig. 9. The top panel displays $\rho r^2(|\xi_r| + \ell(\ell+1)|\xi_h|) \propto e_{\rm kin}$ which corresponds – up to a normalization – to $\mathrm{d}E_{\rm kin}/\mathrm{d}r$ where $E_{\rm kin}$ stands for the total kinetic energy of an oscillation mode. The global run of $e_{\rm kin}$ shows the large weight of the deep interior for the kinetic energy of the mode. This behavior is characteristic of all g modes in our models. The expressed central concentration of $e_{\rm kin}$ leads to large values of $E_{\rm kin}$ which, in a quasi-adiabatic sense, explain the small values of $\sigma_{\rm I}$. Even if the positive and negative parts of the work integral do not nearly cancel. The local depression in the amplitude of $e_{\rm kin}$ around $\log P = 21.5$ coincides with the inner edge of the shell-burning region and the occurring abundance bump in carbon (which is also visible in Fig. 3). Mode trapping is usually associated with such features. For a recent study of ZZ Ceti stars addressing this aspect see Gautschy et al. (1996). Here, the effect is so weak, however, that it is not of much relevance for observed properties of GW Vir stars.

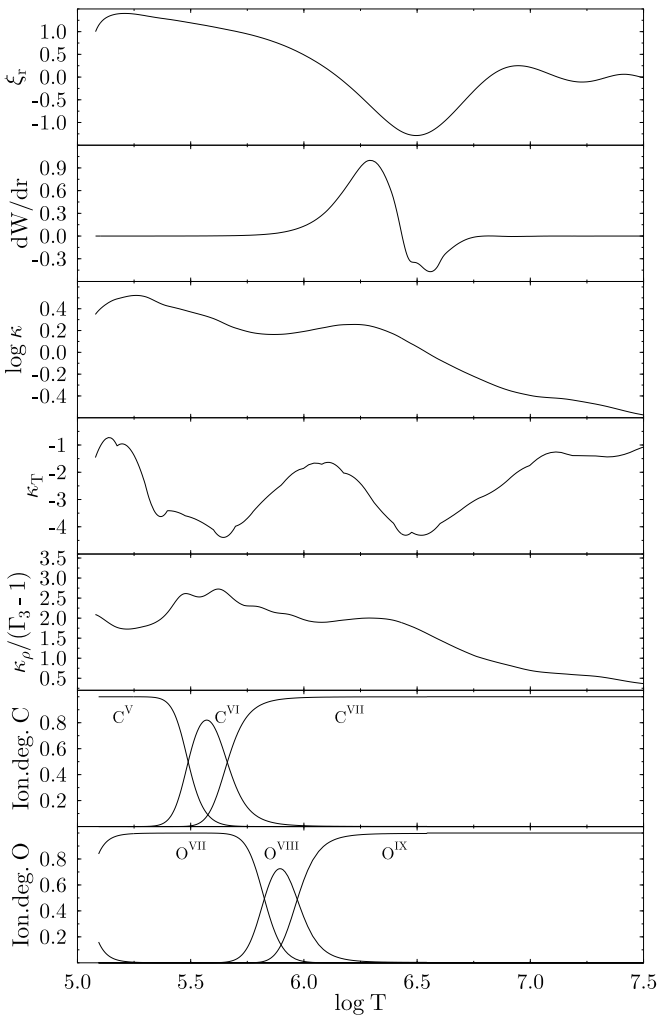

Fig. 10. Eigensolution components and stellar envelope properties of the same model and the same mode as used for Fig. 9. To concentrate on the main driving and damping regions of the oscillations, we restrict the plot to temperatures below $\log T = 7.5$.

The bottom panel of Fig. 9 displays the total work done by the particular oscillation mode. The dominant driving and damping contributions occur between $10 < \log P < 14$ (which corresponds to $5.8 < \log T < 6.8$). The rapid oscillations of the eigenmodes deep in the star lead to a small damping contribution of the total work only. A blow-up of the deep interior shown in the inlet in the lowest panel quantifies this statement.

Fig. 10 shows selected quantities from nonadiabatic nonradial analysis of the $k = 91$ dipole mode as well as from the stellar envelope structure of the underlying model (at $\log g = 6.34$ of the $0.63 M_\odot$ sequence). The top panel depicts the superficial regions of the radial component of the displacement eigenfunction. It demonstrates that most of the spatial oscillations of the eigenfunctions are not significantly involved in the excitation/damping of the mode. The differential work $\mathrm{d}W/\mathrm{d}r$ is seen to be significant in the range $5.8 < \log T < 6.8$. Mode-driving is restricted to the range between 5.8 and 6.4 in $\log T$ which

is in accordance with the opacity bump which reaches a local maximum around $\log T = 6.25$. This feature which is due to the combined effects of L-shell transitions in Fe and K-shell transitions in C, O, and Ne (cf. Seaton et al. 1994) was found to be slightly enhanced (about 20 %, Iglesias et al. 1992) in the new tabulations of stellar opacities (OPAL and OP). Mainly, however, its shape became more pronounced than in the Los-Alamos generation of opacity tables so that it is now more pronounced in $\kappa_{\rm T} = \partial \log \kappa / \partial \log T|\rho$ plots. Fig. 7 demonstrates the influence of strongly reducing the oxygen abundance in the stellar matter. The opacity is globally lowered and so is the bump around $\log T = 6.2$. The sharpness of its ridge on the $\log R$ – $\log T$ plane is, however, hardly influenced. Therefore, the $\kappa_{\rm T}$ run is not very much affected by reducing the O abundance. From the spatial ionization structure of the stellar envelope used for Fig. 10 we see that partial K-shell ionization of carbon might contribute only in the outer parts of the envelope, at temperatures below 10^6 K. Mostly oxygen K-shell ionization and bound-bound transitions in Fe dominate the hotter, more important part of the work integral. We admit that the comparison of the EoS and the opacity data is not fully satisfactory. We were not able to use the OPAL EoS tables with our high C and O abundances for the discussion. Hence, we must rely on our simplified approach which is, hopefully, not too far from reality (cf. Gautschy et al. 1996).

The κ-effect consists of two terms which contribute to driving if

$$\frac{\mathrm{d}}{\mathrm{d}r}\left(\kappa_{\rm T} + \frac{\kappa_\rho}{(\Gamma_3 - 1)}\right) > 0. \qquad (1)$$

From the panel in Fig. 10 which displays the second term in the bracket it is obvious that its gradient is small throughout the driving region and it contributes – if at all – in the low-temperature part only. Below 10^6 K, $\Gamma_3 - 1$ drops noticeable only when the ionization stages O VIII *and* O IX are already considerably populated. At higher temperatures $\Gamma_3 - 1$ is completely flat so that the first term of Eq. 1 controls the driving peak of the differential work. The second term, which is frequently referred to as γ-effect, does not contribute to the overstability of the *g*modes in our GW Vir models.

The period separation and the variation of the imaginary parts as a function of successive radial orders of dipole modes of a selected $0.63 M_\odot$ model are shown in Fig. 11. This particular stellar model is close to the hottest point of the corresponding evolutionary track. Its position is indicated by a horizontal line in the modal diagram of Fig. 5. In the period range between 600 s and 1200 s no obvious sign of mode trapping is visible. In particular, no trapping shows up in the imaginary parts (much in contrast to the way trappings appear in ZZ Ceti stars, cf. Gautschy et al. 1996). The oscillation-period separation ($\Delta\Pi$) as a function of period shows small, seemingly uncorrelated variations on the level one second. The reason is either intrinsic or then reflects the achieved numerical accuracy. The asymptotic formula for low-degree, high-order modes predicts a $\Delta\Pi \approx 23.7$ s which is in reasonable agreement with the full solutions.

Fig. 5 contains the numbers one to four in an outlined font. At these locations we investigated the dependence of the eigen-

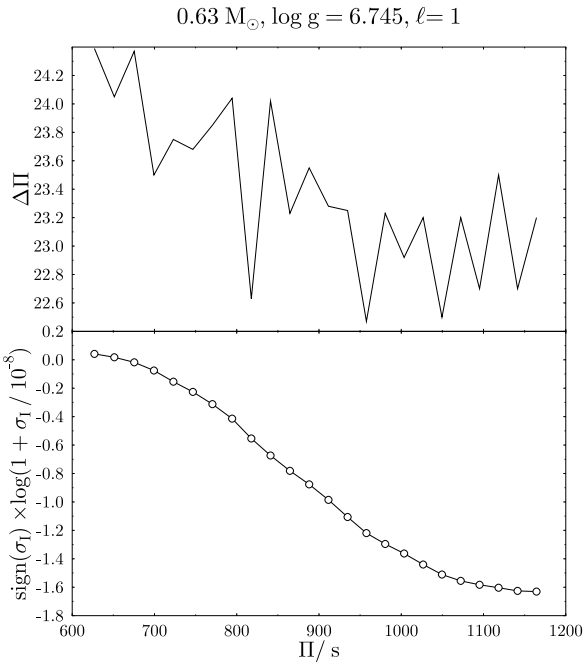

Fig. 11. Period separation and variation of imaginary parts of successive radial orders for the $0.63 M_\odot$ model at $\log g = 6.745$ (indicated by the horizontal line in Fig. 5) for $\ell = 1$.

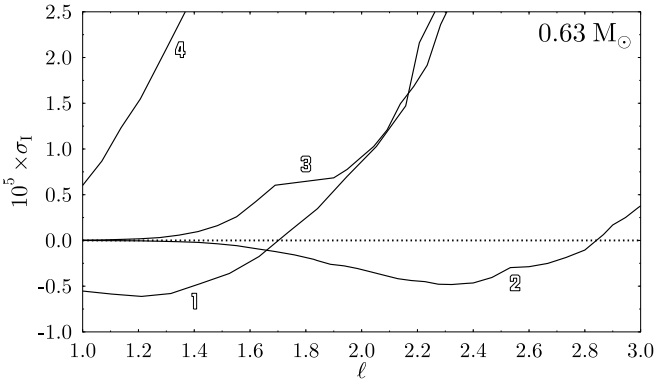

Fig. 12. Reaction of the imaginary parts of eigenvalues of selected $0.63 M_\odot$ models (outlined numbers in Fig. 5) on varying the spherical degree ℓ.

solutions on varying the spherical degree ℓ. Mathematically, ℓ can be treated as a continuous variable; this is what we did to generate Fig. 12. The imaginary parts resulting from such a variation are displayed in Fig. 12. Notice that in contrast to other plots of $\sigma_{\rm I}$ values, the ordinate is on a linear scale. Except at location 2, dipole modes appear to be the most unstable ones. Only at the tip of the instability finger, i.e. at position 2, the marginal instability of dipole modes strengthens towards higher ℓ values and achieves a maximum at about $\ell = 2.4$. From the observational point of view, we expect $\ell = 1$ *and* $\ell = 2$ modes to dominate the oscillation spectra.

The results of our stability analyses do not agree with the Bradley & Dziembowski (1996) results. As far as a compari-

son is possible, the extension of our instability domains and the periods of the most unstable modes agree, however, rather well with the results of Saio (1996): The lengths of the periods of the most unstable modes do not depend sensitively on the particular choice of the oxygen abundance in the driving region. In particular, we do not have postulate neither chemical compositions in the driving region that differ significantly from the one on the stellar surfaces nor increased stellar radii.

7. Conclusions

We computed three sequences of helium-star models (at 0.57, 0.63 and $0.7 M_\odot$) which passed through $\log g - T_{\rm eff}$ the domain which is also populated by GW Vir variables. A large number of mostly dipole oscillation modes were investigated towards their stability behavior with a fully nonadiabatic pulsation code.

GW Vir-like pulsations are driven, as we know for a while already (e.g. Starrfield et al. 1984) by the κ-mechanism of partial ionization of oxygen and carbon. Our Fig. 10 shows the associated opacity bump which peaks around 1.7×10^6 K and which is somewhat enhanced in the new opacity tables (OP: Seaton et al. 1994, OPAL: Iglesias et al. 1992) compared with old data. It appears that not only detailed atomic physics of partial K-shell ionization of carbon, oxygen, and neon are relevant but that spin – orbit coupling of L-shell transitions in iron increases the sharpness of the bump feature additionally. The literature was, in our opinion, never very specific on the particular roles carbon and oxygen played in the *final* picture. According to our EoS, which is not the same as that used in the opacity computations, it should be mainly partial ionization of the K-shell of oxygen which influences the driving of the pulsations. The last ionization level of carbon can only influence the low temperature flank of the driving regime but it cannot *dominate* the driving. This conclusion should of course be tested in detail with consistent EoS and opacity data. As seen in the case of HS2324, carbon and oxygen abundances do not fully determine the excitation problem. For this new variable star we assumed the oxygen abundance by mass to be as low as 0.01 and the hydrogen abundance to make up 20 % in mass. We still found pulsational instabilities. The domain of overstable modes was, however, much narrower than in the case of 'canonical' GW Vir compositions. Nevertheless, we conclude that the stringent composition requirements which were put forth hitherto (e.g. Starrfield et al. 1985, Stanghellini 1991) seem no longer to obtain with the new opacity data. Together with the κ-mechanism the γ-mechanism is frequently brought into play to explain GW Vir variability. In the case of the GW Vir models, the K-shell ionization region of carbon and oxygen reduces Γ_3 only marginally. In our pulsationally overstable models, maximum driving occurs at depths of the last partial ionization stage of oxygen for whichΓ_3 remains essentially constant. The second term of eq. (1) was shown in the third panel from below of Fig. 10. From this we conclude that the γ-effect is not effective for the action of the κ-mechanism in the GW Vir variables – an unusual situation in the theory of pulsating variable stars.

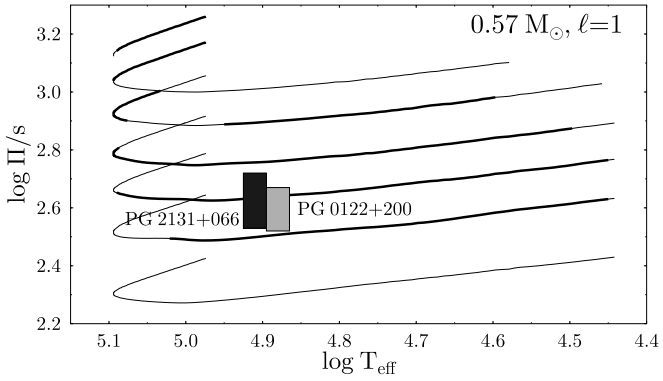

Fig. 13. Period – effective temperature diagram for the ℓ = 1 modes of the $0.57 M_\odot$ model sequence. As before, pulsationally unstable modes are shown with thick lines. For comparison, the two cool GW Vir stars PG2131+066 and PG0122+200 are overlaid with bars spanning the observed period domain and indicating the $T_{\rm eff}$ uncertainty in the other direction.

The instability region for dipole modes is shown with heavy lines in Fig. 2. When translated onto the $\log T_{\rm eff} - \log g$ plane, we find reasonable agreement of the blue edge with observations. As already found in older studies (e.g. Stanghellini et al. 1991), the computed red edge occurs at much lower temperatures than what observations suggest. The $0.57 M_\odot$ models for which this applies in our study show only very weak convection zones close to the surface. A considerable leak of pulsation energy is therefore not likely to occur also with an improved convection-pulsation coupling. To introduce more efficient convection we would have to change the MLT prescription or at least assume a mixing-length parameter which is larger than ours which was chosen to be $\alpha_{\rm MLT}$ = 1.5 pressure scale heights.

Furthermore, the longest periods which we found unstable significantly exceed the longest observed ones (around 2000 s). Lower stellar masses tended to have longer unstable periods. The longest period we encountered is about 9500 s and belongs to the $0.57 M_\odot$ sequence. We noticed that dissipation in the deep interior is only marginal compared with the contributions in the work integral in the temperature range $5.8 < \log T < 6.5$ (cf. Fig. 10). Therefore, we expect the low-temperature region of the stellar interior together with the run of relevant components of the eigensolution therein to be decisive for the overall stability rather than centermost parts with their very short spatial wavelengths.

In Fig. 13 we overlaid the observed oscillation-period range and the spectroscopic temperature calibrations of the cool GW Vir variables PG2131+066 and PG0122+200 on the same oscillation data as displayed in Fig. 6. We are interested in how well they fit into the theoretically determined unstable period domain of the $0.57 M_\odot$ sequence. We refer to the $0.57 M_\odot$ sequence since this is the only of our sequences which shows unstable oscillation modes at sufficiently low effective temperatures. We notice that a significantly smaller period range is observed than what the computations suggest. O'Brien et al. (1996) adopted a period spacing of 21.2 s for PG0122+200. This is smaller than

the 24.1 s from our models. Increasing the stellar mass helps to reduce the discrepancy. Saio's (1996) computations showed that the 'blue edges' of the g-mode instability regions along the white dwarfs' cooling tracks are a function of mass. Increasing the stellar mass shifts the blue edge to lower effective temperatures and hence to lower luminosities ($\log T_{\rm eff} = 5.08$ for $0.58 M_\odot$ and $\log T_{\rm eff} = 5.04$ for $0.60 M_\odot$). Based on the available data we cannot accurately estimate an upper limit of the mass of PG0122+200. However, the hotter the star is the lower is this upper mass limit to guarantee consistency with the very existence of g-mode pulsations.

Adopting our $0.63 M_\odot$ as the closest match with the calibration of RXJ 2117.1+3412 by Vauclair et al. (1993) we found that the long period domain above about 800 s can be explained with unstable modes in our computations. Along the whole $0.63 M_\odot$ sequence we did not find unstable pulsation modes below about 600 s. Therefore, the lowest period at 246 s in the observed power spectrum (Vauclair et al. 1993) lies well below our lower limit. Again, in contrast to the Bradley & Dziembowski (1996) results, we can theoretically recover the observed long periods but occasionally not the short ones. Reducing the model mass would, however, help to reduce the discrepancy.

We did not find mode-trapping cycles in any of our models (cf. the particular case of the $0.63 M_\odot$ model) that are relevant for observed properties of GW Vir variables. The non-smooth run of $\sigma_{\rm I}$ at low luminosities of $0.57 M_\odot$-sequence models indicates some trapping at the composition transition of the extinguishing He shell. Due to the large depth at which this composition transition is located, the corresponding trapping length is much too long to be compatible with observational findings. Therefore, if our thick He envelopes were realistic then elemental diffusion were a necessary ingredient to interpret observed unequal period separations. For thin enough He envelopes, however, as obtained from standard stellar evolution with strong mass loss to shed the H-rich outer layers the superficial position of the μ-barrier due to the He-burning shell serves as a trapping agent.

We have to continue to live with the enigma of seeing about as many stable as pulsating stars in the GW Vir instability domain. This problem is even somewhat aggravated by the results of this study since the particularities of the chemical composition are not necessarily as stringent as believed hitherto. It is conceivable that the heavy element abundance in these objects has a stronger effect than believed up to now. If the iron abundance is low enough, at least in the driving region, then driving might be reduced considerably even if carbon and oxygen abundances are PG1159-like. Therefore, if sedimentation acted long enough to drain enough heavy elements from the driving region some stars might turn stable eventually.

We finish by speculating that mode trapping might help to constrain the evolutionary status of GW Vir variables. Mode trapping occurs at any μ-gradient which builds up. One of them appears at the position of the shell source. This is also the one which is presently believed to be responsible for the observed trapping cycles in some GW Vir variables and which is used to seismically determine the thickness of the He envelopes. Furthermore, elemental diffusion in the strong graviational field of cooling white dwarfs leads to an additional μ-gradient (Dehner & Kawaler 1996) which builds up during the cooling history along the white dwarf sequence. This much more superficial μ-gradient might also reflect and trap oscillation modes. Assume now that we have some mean to identify this superficial μ-gradient then it can serve to distinguish between *first-passers* (on their first passage to the cooling track) and *late shell flashers*. For first-passers at high enough luminosity or low enough surface gravity sedimentation by pressure diffusion has not been very effective yet. This leads to a lack of a superficial μ-barrier. Such stars are expected to show either very regular period spacings which agree well with simple asymptotic formulae if they had very thick He envelopes (as the ones we played with here) or simple trapping cycles that are induced by the shell-burning μ-barrier (e.g. PG1159, see Kawaler & Bradley 1994). Low-luminosity stars or late shell flashers, on the other hand, had enough time for helium to partially purify on top of carbon and oxygen. In such a case, the period separations should show somewhat irregular cyclic depressions. Even a shell flash need not necessarily destroy such a stratification if the star does not loop too far into the low-$T_{\rm eff}$ domain where a large fraction of the envelope becomes convective again.

The discrepancies between our results and those of Bradley & Dziembowski (1996) must possibly be attributed to the numerical treatment of the nonadiabatic oscillation problem rather than to the different stellar models. A pinning down of the origin of the disagreement in the future would be highly desirable.

Acknowledgements. I am indebted to H. Saio for many helpful hints and critical comments throughout the project. K. Werner and S. Dreizler kindly informed me about HS2324 properties prior to their publication. The Swiss National Science Foundation provided financial support through a PROFIL2 fellowship which is gratefully acknowledged.

References

Bergeron P., Wesemael F., Lamontage R., Fontaine G., Saffer R.A., Allard N.F., 1995, ApJ 449, 258
Blöcker T., 1993, Acta Astr. 43, 305
Bradley P.A., Dziembowski W.A., 1996, ApJ 462, 376
Dehner B.T., Kawaler S.D., 1996, preprint
Dreizler S., Werner K., Heber U. 1995, in White Dwarfs, Lecture Notes in Physics 443, eds. D. Koester and K. Werner, Springer, p. 160
Dreizler S., Werner K., Heber U., Engels D., 1996, A&A 309, 820
Gautschy A., Ludwig H.-G., Freytag G., 1996, A&A 311, 493
Iglesias C.A., Rogers F.J., Wilson B.G., 1992, ApJ 397, 717
Kawaler S.D., Bradley P.A. 1994, ApJ 427, 415
Munakata H., Kohyama Y., Itoh N. 1985, ApJ 296, 197; Erratum in ApJ 304, 580
O'Brien M.S., Clemens J.C., Kawaler S.D., Benjamin T., 1996, preprint
Paczyński B., 1970, Acta Astr. 20, 47
Silvotti R., 1996, A&A 309, L23
Saio H. 1996, in Hydrogen Deficient Stars, eds. C.S. Jeffery and U. Heber, ASP Conf. Ser. Vol. 96, p. 361
Seaton M.J., Yu Yan, Mihalas D., Pradhan K. 1994, MNRAS 266, 805
Schönberner D., 1983, ApJ 272, 708
Stanghellini L., Cox A.N., Starrfield S. 1991, ApJ 383, 766
Starrfield S., Cox A.N., Kidman R.B., Pesnell W.D. 1984, ApJ 281, 800

Starrfield S., Cox A.N., Kidman R.B., Pesnell W.D. 1985, ApJ, L23
Vauclair G., Belmonte J.A., Pfeiffer B., Chevreton M., Dolez M., et al. 1993, A&A 267, L35
Werner K., Rauch T., Dreizler S., Heber U. 1995, in Astrophysical Applications of Stellar Pulsation, IAU Coll. 155, eds. R.S. Stobie and P.A. Whitelock, ASP Conf. Ser. Vol. 83, 96
Werner K., Heber U., Hunger K. 1991, A&A 244, 437
Winget D.E., Nather R.E., Clemens J.C., Provencal J., Kleinman S.J., et al. 1991, ApJ 378, 326

This article was processed by the author using Springer-Verlag LaTeX A&A style file *L-AA* version 3.